Hindawi Publishing Corporation
Advances in Optical Technologies
Volume 2008, Article ID 780784, 12 pages
doi:10.1155/2008/780784

Review Article

Tuning of the Optical Properties in Photonic Crystals Made of Macroporous Silicon

Heinz-S. Kitzerow,[1] Heinrich Matthias,[1] Stefan L. Schweizer,[2] Henry M. van Driel,[3] and Ralf B. Wehrspohn[2]

[1] *Department of Chemistry, Faculty of Science, University of Paderborn, 33095 Paderborn, Germany*
[2] *Institute of Physics, Martin-Luther-University Halle-Wittenberg, 06099 Halle, Germany*
[3] *Department of Physics and Institute for Optical Sciences, University of Toronto, Toronto, ON, Canada M5S 1A7*

Correspondence should be addressed to Heinz-S. Kitzerow, heinz.kitzerow@upb.de

Received 9 January 2008; Accepted 11 April 2008

Recommended by D. Lockwood

It is well known that robust and reliable photonic crystal structures can be manufactured with very high precision by electrochemical etching of silicon wafers, which results in two- and three-dimensional photonic crystals made of macroporous silicon. However, tuning of the photonic properties is necessary in order to apply these promising structures in integrated optical devices. For this purpose, different effects have been studied, such as the infiltration with addressable dielectric liquids (liquid crystals), the utilization of Kerr-like nonlinearities of the silicon, or free-charge carrier injection by means of linear (one-photon) and nonlinear (two-photon) absorptions. The present article provides a review, critical discussion, and perspectives about state-of-the-art tuning capabilities.

1. INTRODUCTION

Artificial structures exhibiting a spatially periodic structure with lattice constants comparable to the wavelength of light [1, 2] are extremely promising materials for integrated optical devices. These structures, referred to as photonic crystals [3–11], are characterized by an unusual dispersion relation which might show a photonic band gap (PBG), that is, a frequency range in which the propagation of light is not permitted. Properly designed defects within these structures may serve, for example, as optical waveguides, frequency filters, optical switches, or resonant microcavities with high quality factor, which can be used for low-threshold lasing. Many excellent works have demonstrated the potential capabilities of these structures, but their fabrication is still elaborate.

Electrochemical etching of silicon turned out to be a very reliable and versatile technique to fabricate two-dimensional periodic arrays of macropores [12–15]. Similarly to the method of electrochemical polishing, silicon wafers are dipped into hydrofluoric acid and a DC voltage between the wafer and a counter-electrode is applied. The generation of free charge carriers in the doped silicon is assisted by exposure to infrared radiation. However, in contrast to the common polishing process, the parameters are chosen in a narrow range where the etching process does not lead to flattening of the surface, but instabilities cause the self-organized growth of pores. Spontaneously, the pores tend to arrange in a two-dimensional hexagonal lattice with spacings between $0.5\,\mu$m and $10\,\mu$m. Additional pretreatment of the surface by photolithography can be used to alter the symmetry of the lattice, to create extremely high correlation lengths, and to design the arrangement of defects with very high precision. The depth-to-width ratio of the pores can be as large as 500. In addition, it is possible to modulate the width of the pores along the pore axes by controlling the current through the sample during the growth process, thereby creating even three-dimensional structures [13–15].

In addition to utilizing the benefits of the unusual dispersion relation, it is highly desirable to change the dielectric properties and to control them by external parameters, thereby achieving even a tunable dispersion relation [16–18]. This might be necessary in order to compensate for fabrication tolerances and to fine-tune the properties of the produced photonic crystal, or be motivated by targeting active switching devices. An obvious way to achieve tunable

properties is altering the dielectric susceptibility of the silicon. As usual, the dielectric susceptibility can be expanded in a power series as follows:

$$\chi = \chi^{(1)} + \chi^{(2)}E + \chi^{(3)}EE + \cdots . \quad (1)$$

Thus, linear [$\chi^{(1)}$] or nonlinear effects [$\chi^{(2)}, \chi^{(3)}, \ldots$] may be considered. In addition, the macroporous silicon structures can be filled with a dielectric compound. If the silicon ($\varepsilon = \varepsilon_1$) is infiltrated with a different compound ($\varepsilon = \varepsilon_2$), the most fundamental change is a shift of the average dielectric constant ε_{av}, which is approximately given by the Maxwell-Garnett relation [19]

$$(\varepsilon_{\text{av}} - \varepsilon_1)(\varepsilon_{\text{av}} + 2\varepsilon_1)^{-1} = f_2(\varepsilon_2 - \varepsilon_1)(\varepsilon_2 - 2\varepsilon_1)^{-1}, \quad (2)$$

where f_2 is the volume fraction of component 2. If the denominators in (2) are not too different, the effective refractive index of the composed material is approximately given by

$$n_{\text{eff}} = \left(\Sigma f_i n_i^2\right)^{1/2}, \quad (3)$$

where f_i is the volume fraction of component i of the heterogeneous system. Thus, changing the refractive index of one of the two components has an effect on the properties of the entire structure. However, the influence on the dispersion relation and on the linear and nonlinear photonic properties is much more subtle than a simple change of the average refractive index. Due to their sensitivity to external parameters, liquid crystals proved to be very efficient as a dielectric liquid yielding addressable photonic properties.

In this paper, we would like to review the methods of tuning by means of liquid crystal infiltration (Section 2) as well as all-optical effects that are due to the properties of the silicon (Section 3). The latter effects can be based on charge carrier injection due to one- or two-photon absorption or on Kerr-like nonlinearities (the latter being described by the real part of $\chi^{(3)}$).

2. TUNING BY MEANS OF LIQUID CRYSTAL INFILTRATION

Liquid crystals [20–24] exhibit very sensitive electro- and thermo-optical properties. Filled into the pores of a photonic crystal, they provide the opportunity of adjusting the effective refractive index by external parameters. This method was proposed by Busch and John [25–28] and experimentally demonstrated for colloidal crystals [29–34] before being applied to macroporous silicon [35–46] and other PBG semiconductor structures, including tunable light sources [47–50]. The sensitivity of liquid crystals is due to a preferred uniform alignment of their typically rod-like molecules, which in turn leads to birefringence. The local structure of the least complicated liquid crystalline mesophase, the nematic phase (Figure 1), can be described by the director **n** (a pseudovector) and a scalar order parameter S, which indicate the local molecular alignment (i.e., the optical axis) and the degree of orientational order, respectively. External fields can rotate the optical axis, while an increasing

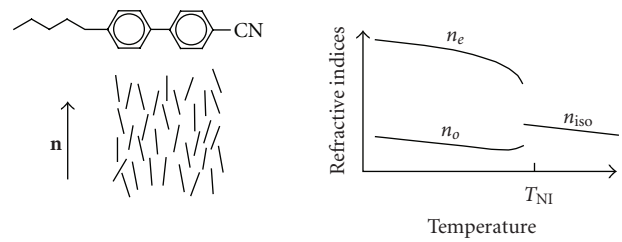

Figure 1: The chemical structure of 4-cyano-4′-pentyl-biphenyl, arrangement of rod-like molecules in the (nonchiral) nematic phase (N), and temperature dependence of the ordinary refractive index n_o (effective for light that is linearly polarized with its electric field perpendicular to the director **n**), the extraordinary refractive index n_e (effective for light that is linearly polarized with its electric field parallel to the director **n**), and the isotropic refractive index n_{iso}.

temperature results in a decreasing order parameter and thus a decreasing birefringence Δn. Typically, the difference $\Delta n = n_e - n_o$ between the extraordinary refractive index n_e and the ordinary refractive index n_o is of the order $\Delta n \approx 0.2$ if the temperature is several Ks below the nematic-isotropic phase transition (clearing temperature). No birefringence appears above the clearing temperature. Thus, relatively large thermally induced changes of the effective refractive index are observed at this phase transition.

Leonard et al. [35] were the first to infiltrate a two-dimensional structure made of macroporous silicon with a liquid crystal and observed changes of the photonic band edge for light propagating in the plane of the silicon wafer. This effect might be very useful for integrated optical waveguides in silicon. Subsequent experiments were focused on three-dimensional (3D) structures consisting of macroporous silicon that are filled with a liquid crystal. The latter structures show also a stop band for light propagating perpendicular to the plane of the wafer. Two-dimensional hexagonal or rectangular arrays of pores with an extremely high aspect ratio (diameter $\leq 1\,\mu$m, depth $\geq 100\,\mu$m) were fabricated by a light-assisted electrochemical etching process using HF [12, 13], and a periodic variation of pore diameter was induced by variation of the electric current during the etching procedure, thereby yielding in a three-dimensional photonic crystal (PhC) [14, 15]. The macroporous structure was evacuated and filled with a liquid crystal. The photonic properties for light propagation along the pore axis were studied by Fourier transform infrared (FTIR) spectroscopy [36–38]. Deuterium-nuclear magnetic resonance (^{2}H-NMR) [36, 37] and fluorescence confocal polarizing microscopy (FCPM) [39–42] were used in order to analyze the director field of the liquid crystal inside the pores.

For example, Figure 2 shows the infrared transmission of samples that show a two-dimensional hexagonal array of pores with a lattice constant $a = 1.5\,\mu$m. Along the pore axis, the diameter of each pore varies periodically between $D_{\text{min}} = (0.76 \pm 0.10)\,\mu$m and $D_{\text{max}} = (1.26 \pm 0.10)\,\mu$m with a lattice constant $b = 2.6\,\mu$m. The pores were filled with the nematic liquid crystal 4-cyano-4′-pentyl-biphenyl (5CB, Figure 1) which shows a clearing temperature of

$T_{NI} = 34°C$. For light propagation along the pore axes, the FTIR transmission spectrum of the silicon-air structure shows a stop band centered at $\lambda = (10.5 \pm 0.5)\,\mu$m. Filling the pores with 5CB decreases the dielectric contrast to silicon and results in a shift of the stop band to $\lambda \approx 12\,\mu$m. The band edge was found to be sensitive to the state of polarization of the incident light. For linearly polarized light, rotation of the sample with respect to the plane of polarization was found to cause a shift of the liquid crystal band edge by $\Delta\lambda \approx 152$ nm (1.61 meV). This effect can quantitatively be explained by the square shape of the pore cross-section, which brakes the threefold symmetry of the hexagonal lattice. Due to the presence of the liquid crystal, the band edge at lower wavelengths ("liquid crystal band" edge) can be tuned by more than 140 nm (1.23 meV) by heating the liquid crystal from 24°C (nematic phase) to 40°C (isotropic liquid phase).

The shift of the photonic band edge towards larger wavelengths indicates an increase of the effective refractive index with increasing temperature. This effect can be explained by a predominantly parallel alignment of the optical axis (director) of the nematic liquid crystal along the pore axis. For a uniform parallel alignment, the effective refractive index of the nematic component corresponds to the ordinary refractive index n_o of 5CB. Increasing the temperature above the clearing point causes an increase to the isotropic value $n_{iso} \approx (1/3n_e^2 + 2/3n_o^2)^{1/2}$, where n_e is the extraordinary refractive index of the liquid crystal ($n_e > n_o$). For a very crude approximation, the average dielectric constant ε_{av} of the heterogeneous structure can be calculated from the respective dielectric constants [$\varepsilon_{LC}(24°C) = n_o^2$ and $\varepsilon_{LC}(40°C) = n_{iso}^2$] using the Maxwell-Garnett relation (2) [19]. The relative shift of the stop band edge towards larger wavelengths corresponds approximately to the relative increase of the average refractive index by ≈ 0.65%. However, more precise analysis of the data shown in Figure 2 indicates that the shift of the two band edges is not the same (the shift of the left band edge is larger). The reason for the difference is that the overlap of the electric field with the pores is different at the two band edges (it is larger at the short wavelength edge), therefore changes of the refractive index in the pores translate into different shifts of the band edge. This is correctly predicted by the calculated dispersion relation shown in the right part of Figure 2, but cannot be explained by the Maxwell-Garnett relation [36].

Planar microcavities inside a 3D photonic crystal appear when the pore diameter is periodically modulated along the pore axis, stays constant within a defect layer, and is continued to vary periodically. Figure 3 shows a structure where a defect layer is embedded between five periodic modulations of the pore diameter. The pores are arranged in a 2D square lattice with a lattice constant of $a = 2\,\mu$m. The pore width varies along the pore axis between $D_{min} = 0.92\,\mu$m and $D_{max} = 1.55\,\mu$m. The length of a modulation is $b = 2.58\,\mu$m. The defect has a length of $l = 2.65\,\mu$m and pore diameters $D_{def} = 0.82\,\mu$m. Within the defect layer, the filling fraction of the liquid crystal is $\xi_{def} = 0.17$. For infrared radiation propagating along the pore axes, a fundamental stop gap at around 13 μm and a second stop gap at around 7 μm are expected from calculations using the plane wave approximation [51]. The experiment shows a transmission peak at $\lambda = 7.184\,\mu$m in the center of the second stop band, which can be attributed to a localized defect mode. Filling the structure with the liquid crystal 4-cyano-4′-pentyl-biphenyl (5CB, Merck) at 24°C causes a spectral red-shift of the stop band. Together with the stop band, the wavelength of the defect state is shifted by 191 nm to $\lambda = 7.375\,\mu$m. An additional shift of $\Delta\lambda = 20$ nm to $\lambda = 7.395\,\mu$m is observed when the liquid crystal is heated from 24°C (nematic phase) to 40°C (isotropic liquid phase). Again, the shift towards larger wavelengths indicates an increase of the effective refractive index n_{eff} of the liquid crystal with increasing temperature and can be attributed to the transition from an initially parallel aligned nematic phase ($n_{LC,eff} = n_o$) to the isotropic state ($n_{LC,eff} = n_{iso}$). During continuous variation of the temperature, a distinct step by 20 nm is observed at the phase transition from the nematic to the isotropic phase. The quality factor Q of the investigated structure, $Q = \lambda/\delta\lambda = 52$, is rather small and thus the shift by 20 nm appears to be small compared to the spectral width of the defect mode. However, the same order of magnitude of the temperature-induced wavelength shift can be expected for structures with a much higher quality factor and might be quite large compared to the band width of the defect mode.

Comparison of experimental ^{2}H-NMR results and calculated spectra (Figure 4) confirms a parallel (P) alignment of the director along the pore axis for substrates that were treated like the samples described above. However, also an anchoring of the director perpendicular to the silicon surfaces ("homeotropic" anchoring) can be achieved if the silicon wafer is cleaned with an ultrasonic bath and a plasma-cleaner and subsequently pretreated with *N*,*N*-dimethyl-*n*-octadecyl-3-aminopropyl-trimethoxysilyl chloride (DMOAP). NMR data indicate the appearance of an escaped radial (ER) director field in the latter case.

For the first time, optical microscopic studies of the director field in pores with a spatially periodic diameter variation could be achieved by means of a nematic liquid crystal polymer that shows a glass-like nematic state at room temperature [39, 40]. For fluorescence polarizing microscopy, the polymer was doped with *N*,*N*′-bis(2,5-di-tert-butylphenyl)-3,4,9,10-perylene-carboximide (BTBP). After filling the photonic crystal in vacuum, the sample was annealed in the nematic phase at 120°C for 24 hours and subsequently cooled to room temperature, thereby freezing the director in the glassy state. The silicon wafer was dissolved in concentrated aqueous KOH solution and the remaining isolated polymer rods were washed and investigated by fluorescence confocal polarizing microscopy (FCPM). The transition dipole moment of the dichroic dye BTBP is oriented along the local director of the liquid crystal host. The incident laser beam (488 nm, Ar^+) and the emitted light pass a polarizer, which implies that the intensity of the detected light scales as $\mathbf{I} \propto \cos^4\alpha$ for an angle α between the local director and the electric field vector of the polarized light. Thus, the local fluorescence intensity indicates the local orientation of the liquid crystal director with very high sensitivity. For a template with homeotropic anchoring and

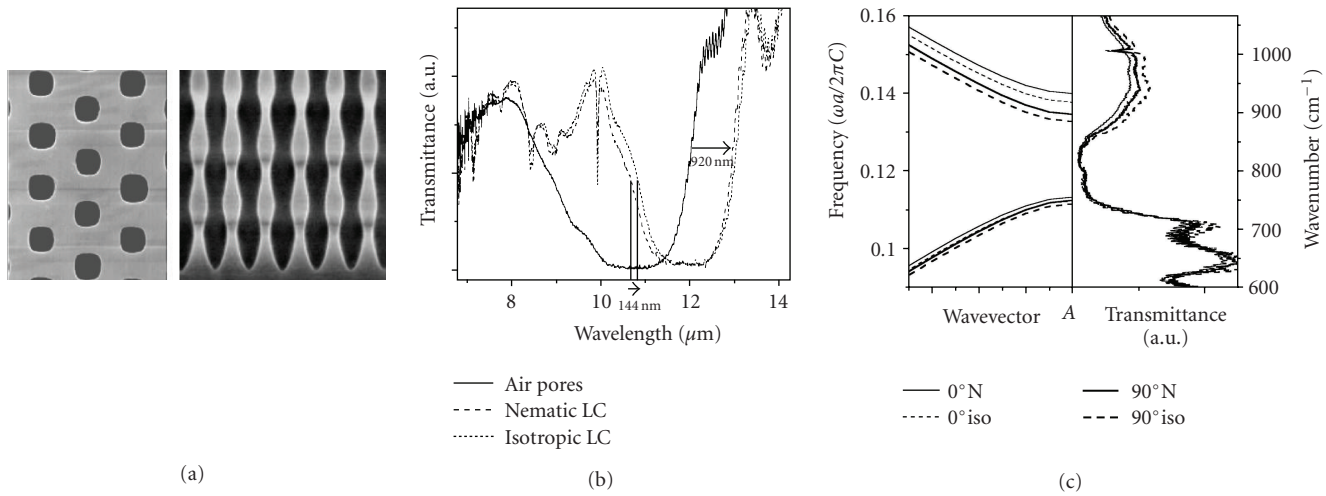

FIGURE 2: (a) SEM top-view and side-view of a photonic crystal made of macroporous silicon containing a two-dimensional hexagonal array of pores with periodically modulated diameter. (b) Transmission spectra of the same photonic crystal for light propagation along the pore axes if the sample is filled with (—) air, (- - -) 5CB in its nematic phase, and (· · ·) 5CB in its isotropic liquid state, respectively. (c) Comparison of the calculated dispersion relation using the plane wave approximation and the experimental spectra. For details, see [36].

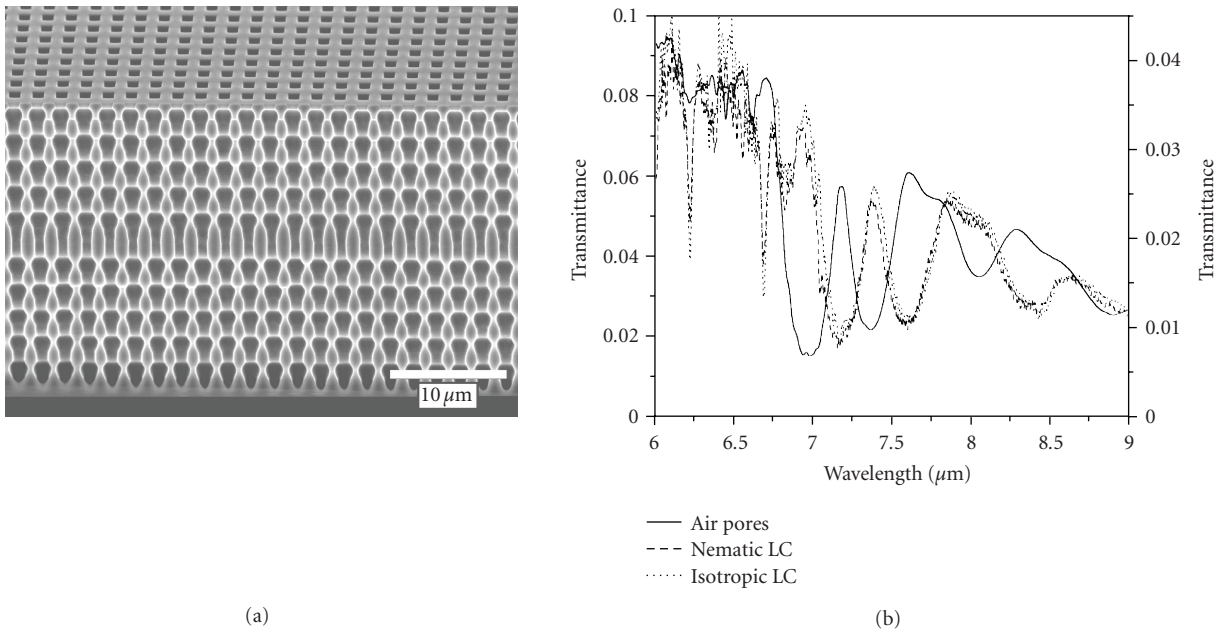

FIGURE 3: (a) SEM image (bird's eye view) of a silicon structure with modulated pores including a planar defect layer without modulation. (b) Transmission spectra of this structure if the sample is filled with (—) air, (- - -) 5CB in its nematic phase, and (· · ·) 5CB in its isotropic liquid state, respectively. For details, see [38].

a sine-like variation of the pore diameter between 2.2 μm and 3.3 μm at a modulation period of 11 μm, the FCPM images of the nematic glass needles (Figure 5) indicate an escaped radial director field. Comparison with numerical calculations based on a tensor algorithm [52, 53] reveals some characteristic features that differ from nonmodulated pores. In the cylindrical cavities studied previously, point-like hedgehog and hyperbolic defects appear at random positions and tend to disappear after annealing, due to the attractive forces between defects of opposite topological charges. In contrast, the modulated pores stabilize a periodic array of disclinations. Moreover, disclination loops appear instead of point-like disclinations.

3. ALL-OPTICAL TUNING

Altering the optical properties by optical irradiation has been the subject of intense research efforts related to the potential development of active photonic crystal components. Here, the impact of an optical pump beam on a photonic crystal

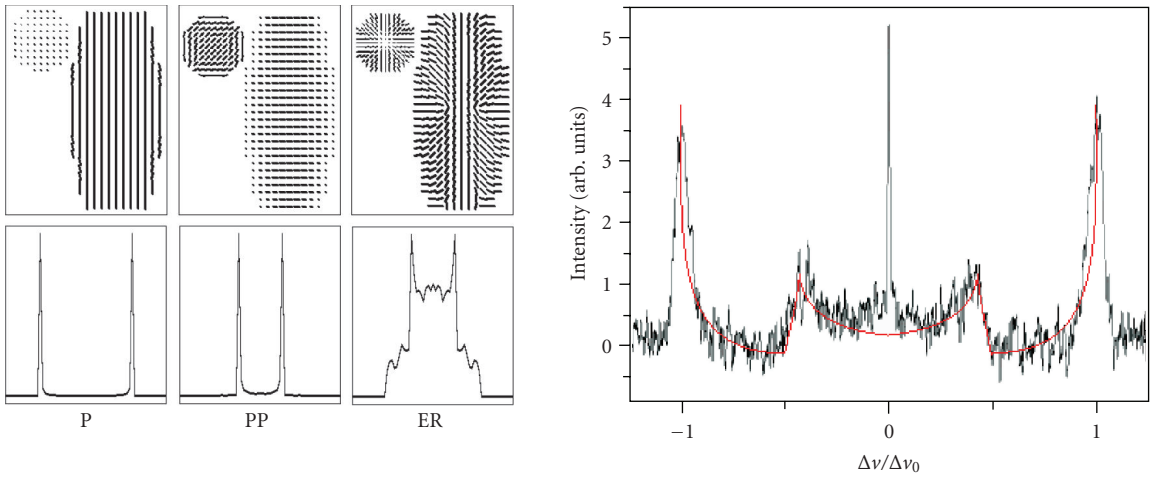

(a) (b)

FIGURE 4: (a) Schematic relation between parallel (P), planar polar (PP), or escaped radial (ER) director fields and the respective ^{2}H-NMR-lineshapes. (b) ^{2}H-NMR spectrum of α-deuterated 5CB in cylindrical pores with perpendicular anchoring [thin line: spectrum expected for an escaped radial (ER) structure with weak anchoring]. For details, see [36, 37].

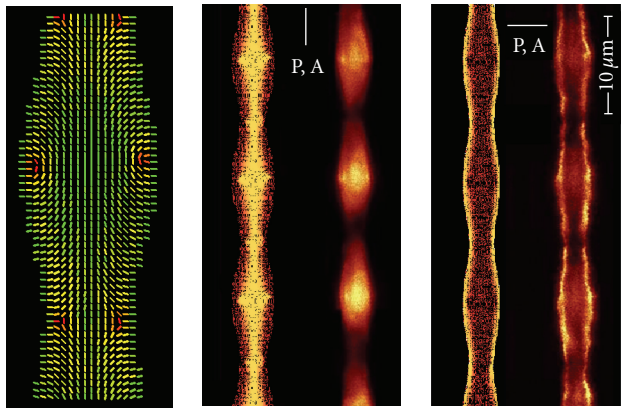

(a) (b) (c)

FIGURE 5: (a) Nematic escaped radial (ER) director field, calculated using the algorithm described in [52, 53]. (b) Theoretical and experimental fluorescent confocal polarizing microscopy (FCPM) images for polarized light with its electric field parallel to the tube axis. (c) Theoretical and experimental FCPM images for polarized light with its electric field perpendicular to the tube axis. For details, see [39].

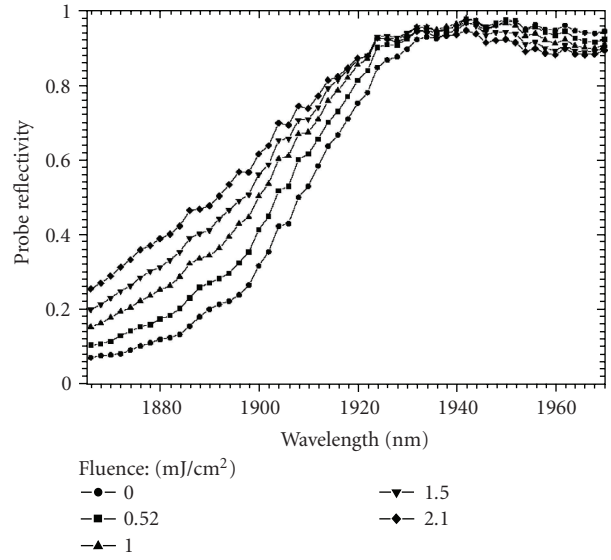

FIGURE 6: Variation of the air band edge of the silicon photon crystal following optical pumping by a 300 fs, 800 nm pulse of variable fluence.

consisting of a two-dimensional array of macropores in silicon [54–59] is reviewed. Figure 7(a) shows a sketch of such a crystal with photo-electrochemically etched straight pores with an aspect ratio of 100 [8, 12, 14]. If the photon energy ($\hbar\omega_p$) of the pump beam is larger than the electronic band gap of silicon, absorption causes a free charge carrier generation in the semiconductor which in turn changes the dielectric constant due to the Drude relation [54] (Section 3.1). These free carriers, generated by photon absorption, can be injected either by a single photon absorption or, in the presence of very high pump intensities, by two-photon absorption. In contrast to the changes achieved by liquid crystal reorientation, this direct optical addressing of the silicon is very fast. Whereas the former occurs on time scales ranging from milliseconds to seconds, the optical tuning takes place in the subpicosecond regime.

Because of the centrosymmetric space group of silicon, bulk-contributions corresponding to the second-order nonlinear susceptibility $\chi^{(2)}$ are ruled out, but surface effects and third-order, that is, Kerr-like nonlinearities, corresponding to $\chi^{(3)}$ can be found. In addition, two-photon absorption of photons with low energy can cause a charge carrier injection

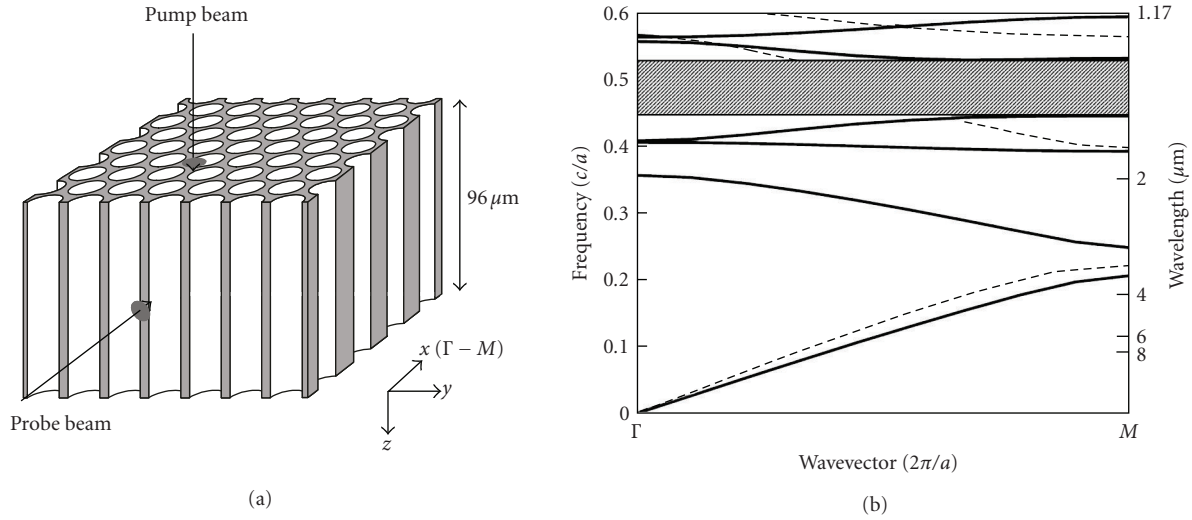

Figure 7: (a) The 2D Si photonic crystal showing pump-probe beam geometry. The probe beam is incident along the Γ-*M* direction. (b) Band structure of the photonic crystal for the Γ-*M* direction. The solid and dashed lines correspond to *E* and *H* polarized lights, respectively.

like the one-photon absorption of photons with high energy. Silicon has an indirect band gap of 1.1 eV ($\lambda = 1.1\,\mu$m) at 295 K and a direct band gap of 3.5 eV ($\lambda = 355$ nm). Thus, a relatively weak phonon-assisted linear absorption or a two-photon one occurs across the visible and near infrared. If the pump intensity is sufficiently high, nonlinear optical effects can cause changes of the dielectric constant even for photon energies that are smaller than the electronic band gap of silicon [55].

3.1. Charge carrier injection by one-photon absorption

To explore the influence of an electron-hole-plasma, a high density of carriers in a native macroporous silicon sample had been optically injected using optical techniques and by this monitoring the shift of a stop-gap edge [54]. As the (indirect band gap) absorption edge of silicon is at 1.1 μm for room temperature, electron-hole pairs can be efficiently produced at shorter wavelengths. The presence of the high density (N) carriers is expected to alter the real part of the dielectric constant ε at probe frequency ω through the expression

$$\varepsilon = \varepsilon_{\mathrm{Si}} - \frac{Ne^2}{\varepsilon_0 \omega^2 m^*}, \tag{4}$$

where $\varepsilon_{\mathrm{Si}}$ (11.9) is the quiescent dielectric constant of silicon, ε_0 is the permittivity of free space, and m^* is the optical effective mass of the electrons and holes. The carrier relaxation rate (~6 THz) has been neglected in comparison with the probing frequencies of interest. In the infrared region of the spectrum for wavelengths between 1 μm and 5 μm, this is a reasonable approximation. Similarly, the influence of the imaginary part of the dielectric constant that would contribute to loss was neglected. From the frequency dependence in (1) one observes that for probing wavelengths in the near infrared region, changes in the dielectric constant of the order of 10% can be obtained for our peak carrier densities. These substantial changes are expected to modify the location of the band gaps. For the experiments, the lowest stop band was investigated, which occurs in the photonic crystal described above between 1.9 μm and 2.3 μm for *E*-polarized light propagating along the Γ-*M* direction. In particular, the shift of the shorter wavelength band edge was measured. Similar shifts are expected for the longer wavelength band edge. The experimental results were obtained with a parametric generator pumped by a 250 kHz repetition rate Ti-sapphire oscillator/regenerative amplifier which produces 130 fs pulses at 800 nm at an average power of 1.1 W. The signal pulse from the parametric generator is tunable from 1.2 μm to 1.6 μm and the idler pulse is tunable from 2.1 μm to 1.6 μm. Reflection measurements were made using 150 fs pulses with center wavelength of 1.9 μm and of sufficient bandwidth to probe the dynamical behavior of this edge. The pulses were focused onto the silicon photonic crystal with fluence per pulse up to ~2 m J cm^{-2}. Simple estimates based on anticipated absorption properties of the photonic crystal at this wavelength indicate that the peak density of electron hole pairs is >10^{18} cm^{-3}. The focal spot diameter of the probe beam was 30 μm, reasonably small compared to the ~100 μm spot diameter of the H-polarized pump beam. Figure 6 shows how the probe reflection characteristics change with the fluence of the pump beam.

The major effect of the optical pumping is to shift the band edge to shorter wavelengths as expected since the Drude contribution decreases the dielectric constant of the silicon. Detailed calculations based on absorption characteristics of the photonic crystal at the pump wavelength and the variation of the photonic crystal dispersion curves with injected carrier density are in agreement with the maximum shift of about 30 nm (at the 3 dB point) that is observed here. Indeed, the shift of the edge scales linearly with the pump fluence, or injected carrier density, as expected theoretically. It should be noted however that the shift of the edge is not

rigid. The shift is less for higher values of the reflectivity. This is presumably related to the fact that the 800 nm pump radiation is inhomogeneously absorbed, with an absorption depth of a few microns. In the spectral range near the peak value of the reflectivity associated with a stop gap, the reflectivity originates from lattice planes over a considerable depth within the crystal. In contrast, Fresnel reflectivity of the surface region dictates the reflection characteristics in the spectral range with higher transmission. To overcome this problem, other pumping schemes have to be used.

It was also possible to time resolve the reflectivity behavior by monitoring the probe reflectivity of the band edge as a function of delay between the probe and pump beams. Not surprisingly, the probe reflectivity change is virtually complete within the duration of the pump beam as charge carriers accumulate in the silicon. However, the recovery of the induced change occurs on a much longer time scale (at least nanoseconds) in our photonic crystal reflecting the electron-hole carrier recombination characteristics.

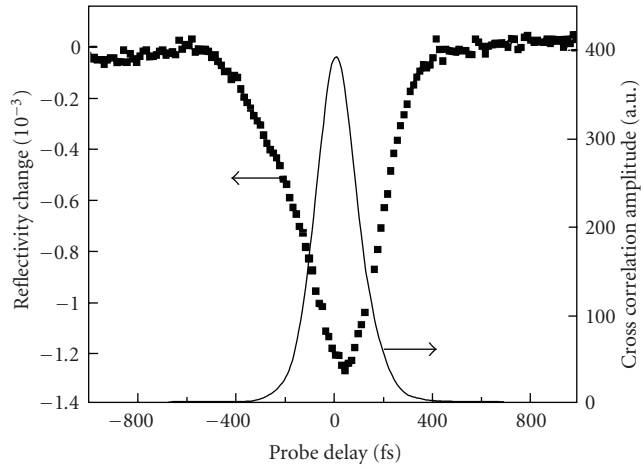

Figure 8: Temporal response of reflectivity change at the 1.3 μm band edge when the PhC is pumped with a 2.0 μm pulse at 17.6 GW/cm^2. Also shown is the cross-correlation trace of the pump and probe pulses.

3.2. Tuning by Kerr-like optical nonlinearities

The Kerr effect was used to tune the short wavelength edge of a photonic band gap. In these experiments, a 2D photonic crystal was used to demonstrate the all optical tuning. Both the short wavelength edge (1.3 μm) and the long wavelength edge (1.6 μm) could be redshifted by the Kerr effect ($\chi^{(3)}$). But for high pump intensities, the two-photon absorption was significantly generating free carriers, leading to a blueshift of the photonic band edge via the Drude contribution to $\chi^{(1)}$.

The 2D silicon PhC sample has a triangular lattice arrangement of 560 nm diameter, 96 μm deep air holes with a pitch, a, equal to 700 nm. Figure 7(a) shows a real space view of the sample while Figure 7(b) illustrates the photonic band structure for the Γ-M direction, which is normal to a face of the PhC. Of particular interest is the third stop gap for E-polarized (E-field parallel to the pore axis) light. Lying between 1.3 μm and 1.6 μm, this gap falls between two dielectric bands that are sensitive to changes in the silicon refractive index. The purpose was to optically induce changes to the two edges with idler pulses from the parametric generator and probe these changes via time-resolved reflectivity of the signal pulses. Note that, because of the link between the signal and idler wavelengths, different pump wavelengths (2.0 μm for a 1.3 μm probe; 1.76 μm for a 1.6 μm probe) must be used when the probe wavelength is changed. However, as will be shown in what follows, small changes in the pump wavelength can lead to significant changes in the induced optical processes.

Figure 8 shows the time-dependent change in reflectivity at 1.3 μm for a 2.0 μm pump pulse and the cross-correlation trace of both pulses. The pump and probe intensities are 17.6 and 0.5 GW/cm^2, respectively. The decrease in reflectivity is consistent with a redshift of the band edge due to a positive nondegenerate Kerr index. The FWHM of the reflectivity trace is 365 $\pm$ 10 fs which is 1.83 times larger than the pump-probe cross-correlation width as measured by sum frequency generation in a beta-barium borate (BBO) crystal. This difference can be explained in terms of pump and probe beam transit time effects in the PhC as discussed above. Indeed, from the pump group velocity and probe spot size, one can deduce that the reflected probe pulse is delayed by 110 fs within the PhC sample. After these effects are taken into account, the intrinsic interaction times are essentially pulse width limited, consistent with the Kerr effect.

One can estimate a value for the nondegenerate Kerr coefficient n_2 in the silicon PhC from the relation [55]

$$\Delta R = \frac{dR}{d\lambda}\frac{d\lambda}{dn} n_2 \frac{1 - R_u}{f} I_0, \tag{5}$$

where I_0 is the incident intensity, f is the filling fraction, and R_u is the reflectivity of the sample. The experimental values of the steepness of the band edge reflectivity, $dR/d\lambda = 0.04\,\text{nm}^{-1}$, and the differential change in band edge wavelength with refractive index, $d\lambda/dn = 174$ nm, are relatively large. Thus, induced reflectivity changes in the vicinity of the 1.3 μm band edge are found to be 70 times more sensitive than that in bulk materials for the same refractive index change, a degree of leverage also noted by others [54, 60]. Indeed, when the PhC is replaced by bulk crystalline silicon, *no change* in reflectivity is observed for the range of pump intensity.

The inset to Figure 9 shows there is good correlation between the change in probe reflectivity and the steepness of the band edge reflectivity (measured separately) at different wavelengths and for a range of pump intensities. Figure 9 shows the change in reflectivity with pump intensity at zero time delay. The linear dependence is consistent with the Kerr effect and the nondegenerate Kerr index is estimated to be 5.2×10^{-15} cm^2/W. This is within an order of magnitude of the degenerate Kerr index reported [61, 62] at 1.27 μm and 1.54 μm and represents reasonable agreement considering uncertainty in the lateral position (x) of the pump pulse and its intensity at the probe location. It should also be noted that

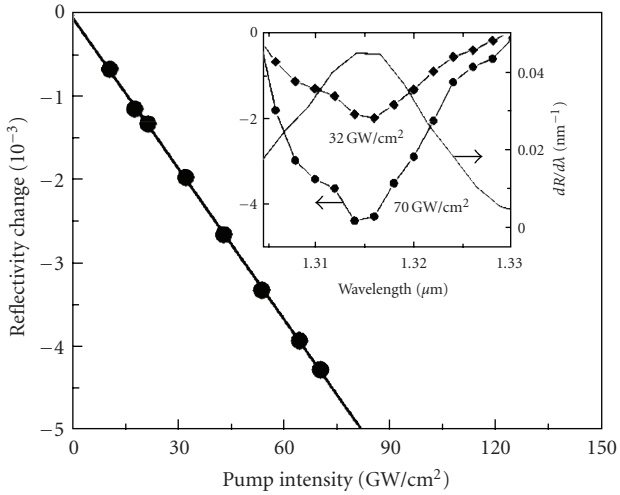

Figure 9: Dependence of probe reflectivity change at 1.316 μm on pump intensity at zero delay. The inset shows the spectral characteristic of reflectivity change at the 1.3 μm band edge at zero delay for different pump intensities at 2.0 μm. Also shown in the inset is the $dR/d\lambda$ curve, which measures the steepness of the band edge reflectivity.

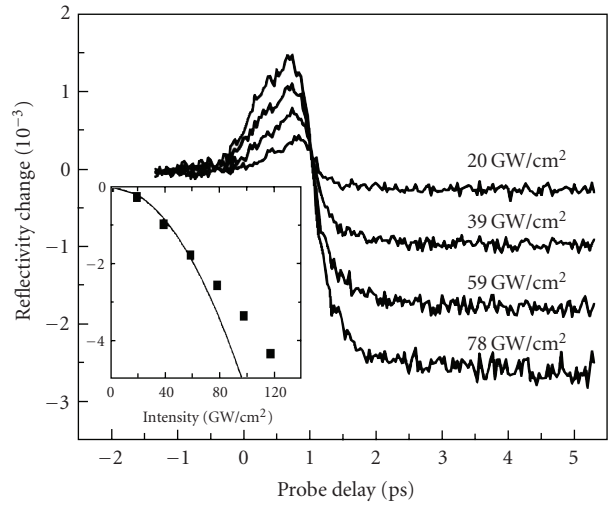

Figure 10: Temporal response of the reflectivity change at the 1.6 μm band edge for different pump intensities at 1.76 μm. The inset shows the dependence of the carrier-induced reflectivity change on pump intensity for low pump powers.

linear scattering losses as the pump pulse propagates through the PhC along the pore axis have not been taken into account.

3.3. Tuning by Kerr-like nonlinearities and two-photon absorption

In general, overall pulse-width limited response can only be achieved using nonresonant, nonlinear induced changes to material optical properties such as the optical Kerr effect (a third-order nonlinearity). In this case, the change in refractive index for a probe beam is given by

$$\Delta n = n_2 I, \tag{6}$$

where I is the intensity of the pump beam and n_2 is the Kerr coefficient associated with the pump and probe frequencies. If the probe light intensity is limited to values like in the experiment of Leonard et al. [54], the imaginary terms in the dielectric function arising from free-carrier absorption and intervalence-band absorption are very small.

Results from experiments used to probe the 1.6 μm band edge when the sample is pumped with 1.76 μm pulses are illustrated in Figure 10, which shows the temporal response of the change in probe reflectivity at different pump intensities for a probe intensity of 0.13 GW/cm^2. There is an initial increase and decrease in probe reflectivity on a subpicosecond time scale followed by a response that decays on a time scale of 900 picoseconds and partially masks the Kerr effect near zero delay. At this band edge, the subpicosecond behavior is consistent with a Kerr effect similar to the previous experiments. The long time response could possibly be due to thermal or Drude contributions to the dielectric constant due to the generation of free carriers. Using a peak pump intensity of 120 GW/cm^2 and a 0.8 cm/GW two-photon absorption coefficient [61, 62] for 1.55 μm as an upper limit, one can estimate the surface peak carrier density to be $<10^{19}$ cm^{-3} and the maximum change in temperature to be <0.15 K. From the thermo-optic coefficient $\partial n/\partial T \approx 1 \times 10^{-4}$ K^{-1} at the probe wavelength [63], the change in silicon refractive index is on the order of 10^{-5} and the (positive) induced change in reflectivity is expected to be about the same. From free carrier (Drude) contributions to the refractive index at the probe wavelength, changes to the imaginary part of the dielectric constant are about 2 orders of magnitude smaller than that of the real part [64], which is about -10^{-3}. Hence, free carrier absorption of the probe pulse as well as thermally induced changes can be neglected in what follows and the change in reflectivity is ascribed to changes in the real part of the dielectric constant due to Drude effects.

At low pump powers, the change in probe reflectivity scales quadratically with pump intensity. This can be explained by free carrier generation due to two-photon absorption, with the charge carrier density N being given by

$$N(z) = \frac{\sqrt{\pi}\beta\tau_p}{4\hbar\omega_p\sqrt{\ln 2}} I^2(z), \tag{7}$$

where β is the two-photon absorption coefficient, τ_p is the temporal FWHM pulse width of the pump pulses, and ω_p is the pump frequency. However, at higher pump intensities, there is an apparent deviation from this quadratic dependence (see inset in Figure 10) due to pump saturation effects, since the pump intensity I varies along the z-direction as

$$I(z) = \frac{(1-R_u)I_0}{f + \beta z(1-R_u)I_0}, \tag{8}$$

according to attenuation by two-photon absorption. With increasing intensity in a two-photon absorption process, an increasing fraction of the carriers are created closer to the

Table 1: Spectral shifts and switching speeds of the different effects described in Sections 2 and 3.

Effect	Initial frequency ν (Hz)	Frequency shift $\delta\nu$ or refractive index shift δn/control parameter	Relative frequency shift $\lvert\delta\nu\rvert/\nu$	Time constant (s)
Temperature-induced shift of the "silicon" band edge in a liquid crystal-infiltrated structure [36].	$2.32 \cdot 10^{13}$	$\delta\nu/\delta T = -1.68 \cdot 10^{11}$ Hz/16°C	0.72%	
Temperature-induced shift of the "liquid crystal" band edge in a liquid crystal-infiltrated structure [36].	$2.81 \cdot 10^{13}$	$\delta\nu/\delta T = -3.74 \cdot 10^{11}$ Hz/16°C	1.33%	$\approx 10^{-3}$
Temperature-induced shift of the microcavity resonance in a liquid crystal-infiltrated structure [38].	$4.05 \cdot 10^{13}$	$\delta\nu/\delta T = -1.56 \cdot 10^{11}$ Hz/1°C	0.39%	
Temperature-induced shift of the PL emission frequency in an Er-doped liquid crystal-infiltrated structure [46].	$1.93 \cdot 10^{14}$	$\delta\nu/\delta T = -8.70 \cdot 10^{11}$ Hz/23°C	0.45%	
Free charge carrier injection induced by one-photon absorption [54].	$1.58 \cdot 10^{14}$	$\delta\nu/\delta T = -2.53 \cdot 10^{12}$ Hz/(2.1 ± 0.4) m J/cm^2	1.60%	$\approx 10^{-6}$
Tuning by Kerr-like nonlinearities [55].		$\delta n \approx 10^{-3}$		Instantaneous (10^{-13})

surface where the pump pulse enters and the probe region develops a reduced and increasingly nonuniform carrier density. It can be estimated that at a depth of 60 μm, the expected saturation pump intensity is about an order of magnitude larger than the maximum pump intensity used in this setup. The carrier lifetime of 900 picoseconds is most likely associated with surface recombination within the PhC sample with its large internal surface area.

The reflectivity change due to the Drude effect is given by

$$\Delta R = \frac{dR}{d\lambda}\frac{d\lambda}{dn}\frac{e^2}{2n_0\omega_r^2 m^* \varepsilon_0}\frac{\sqrt{\pi}\beta\tau_p}{4\hbar\omega_p\sqrt{\ln 2}}I^2(z), \qquad (9)$$

where ω_r is the probe frequency, m^* is the effective optical mass of the electrons and holes ($= 0.16\, m_0$), and ε_0 is the permittivity of free space. Thus, from the low intensity behavior in the inset to Figure 10, the two-photon absorption coefficient, β, can be estimated to be 0.02 cm/GW, which is within an order of magnitude but smaller than that reported [61, 65] for wavelengths near 1.55 μm. For the 2 μm pump wavelength, the upper limit for β is estimated to be 2×10^{-3} cm/GW from the signal to noise and the fact that no measurable long-lived response at the highest pump intensity used is observed. This value is an order of magnitude smaller than what is determined at 1.76 μm and it is not a surprise since β is expected to decrease rapidly with increasing wavelength as the indirect gap edge is approached.

4. SUMMARY

In conclusion, either the infiltration of macroporous silicon with liquid crystals and subsequent control of the thermodynamic variables or the use of light absorption of Kerr-like optical nonlinearities can be used to achieve tunable properties in photonic crystals made of macroporous silicon. For both methods, the relative frequency shift of photonic bands, band edges, or resonance frequencies of microcavities is roughly of the order of 1% of the absolute frequency (Table 1). The effect is limited, but can nevertheless be much larger than the linewidth of modes to be tuned, since microresonators with very large Q factors can be fabricated. The methods summarized in Sections 2 and 3 may find different applications. The use of liquid crystals has the advantage that the control parameters temperature and electric fields are easily available. However, the greatest disadvantage is probably the limited speed of director

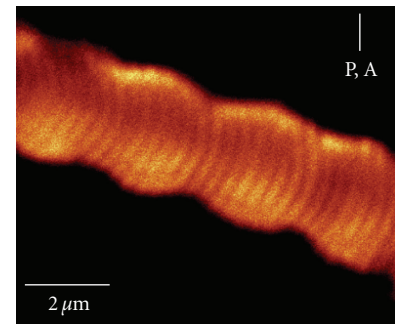

Figure 11: FCPM image of a cholesteric cylinder with perpendicular anchoring and a helix pitch smaller than the cylinder diameter. The regular fringes are perpendicular to the pitch axis and their distance corresponds to one half of the pitch. For further details, see [41].

reorientation, which corresponds to time constants in the millisecond range. In contrast, absorption and nonlinear effects lead to very fast changes of the photonic properties (with time constants below 1 picosecond) and can be used for all-optical switching. However, very large intensities are required for the nonlinear optical effects.

Besides further technical developments that make use of the effects studied, so far, a couple of novel, fundamentally interesting systems deserve to be explored in more detail:

(1) Chiral liquid crystals: cholesteric phases and blue phases [20–24] show a helical superstructure of the local alignment, thereby leading to a spatially periodic director field $\mathbf{n}(\mathbf{r})$. This intrinsic periodicity can be combined with two-dimensional arrays of pores, thereby leading to novel three-dimensional heterogeneous structures [41]. As an example, Figure 11 shows the FCPM image of a sample which shows an inherent periodicity within the pores. Such structures may show enhanced nonlinear optical effects or may be used for switching between a three-dimensional and a two-dimensional periodicity of the optical density. Additional work on these systems is in progress.

(2) Liquid crystals can exhibit both second- and third-order optical nonlinearity. Thus, infiltration of photonic crystals with liquid crystals that exhibit large $\chi^{(2)}$- or $\chi^{(3)}$-values may be used for frequency conversion or all-optical switching, respectively. A considerable enhancement of second harmonic generation (SHG) intensity is known to appear in spatially periodic structures, where both the fundamental frequency and the second harmonic are close to photonic stop bands [66, 67]. In addition, suitable liquid crystals are known for their giant optical nonlinearity (GON) [68], that is, a huge Kerr effect which is due to collective reorientation of the liquid crystal molecules induced by the optical electric field strength.

Fundamental studies of these effects in the environment of a silicon photonic crystal appear to be challenging. In conclusion, the development of tunable photonic crystals based on silicon is still in progress.

ACKNOWLEDGMENTS

This work was supported by the company E. Merck (Darmstadt) with liquid crystals. Also, the funding by the German Research Foundation (KI 411/4 and SPP 1113) and the European Science Foundation (EUROCORES/05-SONS-FP-014) is gratefully acknowledged.

REFERENCES

[1] E. Yablonovitch, "Inhibited spontaneous emission in solid-state physics and electronics," *Physical Review Letters*, vol. 58, no. 20, pp. 2059–2062, 1987.

[2] S. John, "Strong localization of photons in certain disordered dielectric superlattices," *Physical Review Letters*, vol. 58, no. 23, pp. 2486–2489, 1987.

[3] J. D. Joannopoulos, R. D. Meade, and J. N. Winn, *Photonic Crystals: Molding the Flow of Light*, Princeton University Press, Princeton, NJ, USA, 1995.

[4] C. M. Soukoulis, Ed., *Photonic Crystals and Light Localization in the 21st Century*, vol. 563 of *NATO Science Series C: Mathematical and Physical Sciences*, Kluwer Academic Publishers, Dordrecht, The Netherlands, 2001.

[5] S. G. Johnson and J. D. Joannopoulos, *Photonic Crystals: The Road from Theory to Practice*, Kluwer Academic Publishers, Boston, Mass, USA, 2002.

[6] R. E. Slusher and B. J. Eggleton, Eds., *Nonlinear Photonic Crystals*, vol. 10 of *Springer Series in Photonics*, Springer, Berlin, Germany, 2003.

[7] K. Inoue and K. Ohtaka, Eds., *Photonic Crystals: Physics, Fabrication and Applications*, vol. 94 of *Springer Series in Optical Sciences*, Springer, Berlin, Germany, 2004.

[8] K. Busch, S. Lölkes, R. B. Wehrspohn, and H. Föll, Eds., *Photonic Crystals: Advances in Design, Fabrication and Characterization*, Wiley-VCH, Weinheim, Germany, 2004.

[9] K. Sakoda, *Optical Properties of Photonic Crystals*, vol. 80 of *Springer Series in Optical Sciences*, Springer, Berlin, Germany, 2nd edition, 2005.

[10] J.-M. Lourtioz, H. Benisty, V. Berger, J.-M. Gerard, D. Maystre, and A. Tchelnokov, *Photonic Crystals: Towards Nanoscale Photonic Devices*, Springer, Berlin, Germany, 2005.

[11] K. Yasumoto, Ed., *Electromagnetic Theory and Applications for Photonic Crystals*, vol. 102 of *Optical Science and Engineering*, CRC Press, Boca Raton, Fla, USA, 2006.

[12] F. Müller, A. Birner, U. Gösele, V. Lehmann, S. Ottow, and H. Föll, "Structuring of macroporous silicon for applications as photonic crystals," *Journal of Porous Materials*, vol. 7, no. 1, pp. 201–204, 2000.

[13] J. Schilling, F. Müller, S. Matthias, R. B. Wehrspohn, U. Gösele, and K. Busch, "Three-dimensional photonic crystals based on macroporous silicon with modulated pore diameter," *Applied Physics Letters*, vol. 78, no. 9, pp. 1180–1182, 2001.

[14] A. Birner, R. B. Wehrspohn, U. M. Gösele, and K. Busch, "Silicon-based photonic crystals," *Advanced Materials*, vol. 13, no. 6, pp. 377–388, 2001.

[15] S. Matthias, R. Hillebrand, F. Müller, and U. Gösele, "Macroporous silicon: homogeneity investigations and fabrication tolerances of a simple cubic three-dimensional photonic crystal," *Journal of Applied Physics*, vol. 99, no. 11, Article ID 113102, 5 pages, 2006.

[16] P. V. Braun and S. M. Weiss, Eds., *Tuning the Optic Response of Photonic Bandgap Structures III*, vol. 6322 of *Proceedings of the SPIE*, San Diego, Calif, USA, August 2006.

[17] P. M. Fauchet and P. V. Braun, Eds., *Tuning the Optical Response of Photonic Bandgap Structures II*, vol. 5926 of *Proceedings of the SPIE*, San Diego, Calif, USA, July-August 2005.

[18] P. M. Fauchet and P. V. Braun, Eds., *Tuning the Optical Response of Photonic Bandgap Structures*, vol. 5511 of *Proceedings of the SPIE*, Denver, Colo, USA, August 2004.

[19] J. C. M. Garnett, "Colours in metal glasses and in metallic films," *Philosophical Transactions of the Royal Society of London A*, vol. 203, pp. 385–420, 1904.

[20] P. G. de Gennes and J. Prost, *The Physics of Liquid Crystals*, Clarendon Press, Oxford, UK, 2nd edition, 1993.

[21] S. Chandrasekhar, *Liquid Crystals*, Cambridge University Press, Cambridge, UK, 2nd edition, 1992.

[22] S. Kumar, Ed., *Liquid Crystals: Experimental Study of Physical Properties and Phase Transitions*, Cambridge University Press, Cambridge, UK, 2001.

[23] G. P. Crawford and S. Žumer, Eds., *Liquid Crystals in Complex Geometries Formed by Polymer and Porous Networks*, Taylor & Francis, London, UK, 1996.

[24] H.-S. Kitzerow, "The effect of electric fields on blue phases," *Molecular Crystals and Liquid Crystals*, vol. 202, no. 1, pp. 51–83, 1991.

[25] K. Busch and S. John, "Photonic band gap formation in certain self-organizing systems," *Physical Review E*, vol. 58, no. 3, pp. 3896–3908, 1998.

[26] K. Busch and S. John, "Liquid-crystal photonic-band-gap materials: the tunable electromagnetic vacuum," *Physical Review Letters*, vol. 83, no. 5, pp. 967–970, 1999.

[27] S. John and K. Busch, "Photonic bandgap formation and tunability in certain self-organizing systems," *Journal of Lightwave Technology*, vol. 17, no. 11, pp. 1931–1943, 1999.

[28] S. John and K. Busch, "Electro-actively tunable photonic bandgap materials," US patent 6813064, November 2004.

[29] K. Yoshino, Y. Shimoda, Y. Kawagishi, K. Nakayama, and M. Ozaki, "Temperature tuning of the stop band in transmission spectra of liquid-crystal infiltrated synthetic opal as tunable photonic crystal," *Applied Physics Letters*, vol. 75, no. 7, pp. 932–934, 1999.

[30] K. Yoshino, S. Satoh, Y. Shimoda, Y. Kawagishi, K. Nakayama, and M. Ozaki, "Tunable optical stop band and reflection peak in synthetic opal infiltrated with liquid crystal and conducting polymer as photonic crystal," *Japanese Journal of Applied Physics*, vol. 38, no. 8, pp. L961–L963, 1999.

[31] D. Kang, J. E. Maclennan, N. A. Clark, A. A. Zakhidov, and R. H. Baughman, "Electro-optic behavior of liquid-crystal-filled silica opal photonic crystals: effect of liquid-crystal alignment," *Physical Review Letters*, vol. 86, no. 18, pp. 4052–4055, 2001.

[32] G. Mertens, T. Röder, R. Schweins, K. Huber, and H.-S. Kitzerow, "Shift of the photonic band gap in two photonic crystal/liquid crystal composites," *Applied Physics Letters*, vol. 80, no. 11, pp. 1885–1887, 2002.

[33] H.-S. Kitzerow, A. Hoischen, G. Mertens, et al., "Polymer / liquid crystal composites: from polymer-dispersed liquid crystals to tunable photonic crystals," *Polymer Preprints*, vol. 43, no. 2, pp. 534–535, 2002.

[34] H.-S. Kitzerow, "Tunable photonic crystals," *Liquid Crystals Today*, vol. 11, no. 4, pp. 3–7, 2002.

[35] S. W. Leonard, J. P. Mondia, H. M. van Driel, et al., "Tunable two-dimensional photonic crystals using liquid-crystal infiltration," *Physical Review B*, vol. 61, no. 4, pp. R2389–R2392, 2000.

[36] G. Mertens, T. Röder, H. Matthias, et al., "Two- and three-dimensional photonic crystals made of macroporous silicon and liquid crystals," *Applied Physics Letters*, vol. 83, no. 15, pp. 3036–3038, 2003.

[37] G. Mertens, *Anwendung von Flüssigkristallen für abstimmbare photonische Kristalle*, Ph.D. dissertation, University of Paderborn, Paderborn, Germany, 2004.

[38] G. Mertens, R. B. Wehrspohn, H.-S. Kitzerow, S. Matthias, C. Jamois, and U. Gösele, "Tunable defect mode in a three-dimensional photonic crystal," *Applied Physics Letters*, vol. 87, no. 24, Article ID 241108, 3 pages, 2005.

[39] H. Matthias, T. Röder, R. B. Wehrspohn, H.-S. Kitzerow, S. Matthias, and S. J. Picken, "Spatially periodic liquid crystal director field appearing in a photonic crystal template," *Applied Physics Letters*, vol. 87, no. 24, Article ID 241105, 3 pages, 2005.

[40] H.-S. Kitzerow, G. Mertens, H. Matthias, et al., "Director fields of nematic liquid crystals in tunable photonic crystals," in *Tuning the Optical Response of Photonic Bandgap Structures II*, vol. 5926 of *Proceedings of SPIE*, pp. 25–34, San Diego, Calif, USA, July-August 2005.

[41] H. Matthias, S. L. Schweizer, R. B. Wehrspohn, and H.-S. Kitzerow, "Liquid crystal director fields in micropores of photonic crystals," *Journal of Optics A*, vol. 9, no. 9, pp. S389–S395, 2007.

[42] H.-S. Kitzerow, A. Lorenz, and H. Matthias, "Tuneable photonic crystals obtained by liquid crystal infiltration," *Physica Status Solidi (A)*, vol. 204, no. 11, pp. 3754–3767, 2007.

[43] S. M. Weiss, M. Haurylau, and P. M. Fauchet, "Tunable photonic bandgap structures for optical interconnects," *Optical Materials*, vol. 27, no. 5, pp. 740–744, 2005.

[44] S. M. Weiss, H. Ouyang, J. Zhang, and P. M. Fauchet, "Electrical and thermal modulation of silicon photonic bandgap microcavities containing liquid crystals," *Optics Express*, vol. 13, no. 4, pp. 1090–1097, 2005.

[45] M. Haurylau, S. P. Anderson, K. L. Marshall, and P. M. Fauchet, "Electrically tunable silicon 2-D photonic bandgap structures," *IEEE Journal on Selected Topics in Quantum Electronics*, vol. 12, no. 6, pp. 1527–1532, 2006.

[46] S. M. Weiss, J. Zhang, P. M. Fauchet, V. V. Seregin, and J. L. Coffer, "Tunable silicon-based light sources using erbium doped liquid crystals," *Applied Physics Letters*, vol. 90, no. 3, Article ID 031112, 3 pages, 2007.

[47] Ch. Schuller, F. Klopf, J. P. Reithmaier, M. Kamp, and A. Forchel, "Tunable photonic crystals fabricated in III-V semiconductor slab waveguides using infiltrated liquid crystals," *Applied Physics Letters*, vol. 82, no. 17, pp. 2767–2769, 2003.

[48] H.-S. Kitzerow and J. P. Reithmaier, "Tunable photonic crystals using liquid crystals," in *Photonic Crystals: Advances in Design, Fabrication and Characterization*, K. Busch, H. Föll, S. Lölkes, and R. B. Wehrspohn, Eds., chapter 9, pp. 174–197, Wiley-VCH, Weinheim, Germany, 2004.

[49] B. Maune, M. Lončar, J. Witzens, et al., "Liquid-crystal electric tuning of a photonic crystal laser," *Applied Physics Letters*, vol. 85, no. 3, pp. 360–362, 2004.

[50] K. A. Piegdon, H. Matthias, C. Meier, and H.-S. Kitzerow, "Tunable optical properties of photonic crystals and semiconductor microdisks using liquid crystals," in *Emerging Liquid Crystal Technologies III*, vol. 6911 of *Proceedings of SPIE*, pp. 6911–1619, San Jose, Calif, USA, January 2008.

[51] S. G. Johnson and J. D. Joannopoulos, "Block-iterative frequency-domain methods for Maxwell's equations in a planewave basis," *Optics Express*, vol. 8, no. 3, pp. 173–190, 2001.

[52] S. Dickmann, *Numerische Berechnung von Feld und Molekülausrichtung in Flüssigkristallanzeigen*, Ph.D. thesis, University of Karlsruhe, Karlsruhe, Germany, 1994.

[53] H. Mori, E. C. Gartland Jr., J. R. Kelly, and P. J. Bos, "Multidimensional director modeling using the Q tensor representation in a liquid crystal cell and its application to the π cell with patterned electrodes," *Japanese Journal of Applied Physics*, vol. 38, no. 1, pp. 135–146, 1999.

[54] S. W. Leonard, H. M. van Driel, J. Schilling, and R. B. Wehrspohn, "Ultrafast band-edge tuning of a two-dimensional silicon photonic crystal via free-carrier injection," *Physical Review B*, vol. 66, no. 16, Article ID 161102, 4 pages, 2002.

[55] H. W. Tan, H. M. van Driel, S. L. Schweizer, R. B. Wehrspohn, and U. Gösele, "Nonlinear optical tuning of a two-dimensional silicon photonic crystal," *Physical Review B*, vol. 70, no. 20, Article ID 205110, 5 pages, 2004.

[56] H. W. Tan, H. M. van Driel, S. L. Schweizer, and R. B. Wehrspohn, "Influence of eigenmode characteristics on optical tuning of a two-dimensional silicon photonic crystal," *Physical Review B*, vol. 72, no. 16, Article ID 165115, 8 pages, 2005.

[57] S. L. Schweizer, R. B. Wehrspohn, H. W. Tan, and H. M. van Driel, "Nonlinear optical tuning in a 2-D silicon photonic crystal," in *Tuning the Optical Response of Photonic Bandgap Structures II*, vol. 5926 of *Proceedings of SPIE*, pp. 48–56, San Diego, Calif, USA, July-August 2005.

[58] H. W. Tan, H. M. van Driel, S. L. Schweizer, and R. B. Wehrspohn, "Phase and envelope characteristics of ultrashort pulses reflected from a two-dimensional silicon photonic crystal," *Physical Review B*, vol. 74, no. 3, Article ID 035116, 6 pages, 2006.

[59] A. D. Bristow, N. Rotenberg, and H. M. van Driel, "Two-photon absorption and Kerr coefficients of silicon for 850–2200 nm," *Applied Physics Letters*, vol. 90, no. 19, Article ID 191104, 3 pages, 2007.

[60] A. D. Bristow, J.-P. R. Wells, W. H. Fan, et al., "Ultrafast nonlinear response of AlGaAs two-dimensional photonic crystal waveguides," *Applied Physics Letters*, vol. 83, no. 5, pp. 851–853, 2003.

[61] M. Dinu, F. Quochi, and H. Garcia, "Third-order nonlinearities in silicon at telecom wavelengths," *Applied Physics Letters*, vol. 82, no. 18, pp. 2954–2956, 2003.

[62] H. K. Tsang, C. S. Wong, T. K. Liang, et al., "Optical dispersion, two-photon absorption and self-phase modulation in silicon waveguides at 1.5 μm wavelength," *Applied Physics Letters*, vol. 80, no. 3, pp. 416–418, 2002.

[63] K.-H. Hellwege, Ed., *Landolt-Bornstein 17-a*, Springer, Berlin, Germany, 1982.

[64] M. I. Gallant and H. M. van Driel, "Infrared reflectivity probing of thermal and spatial properties of laser-generated carriers in germanium," *Physical Review B*, vol. 26, no. 4, pp. 2133–2146, 1982.

[65] R. W. Boyd, *Nonlinear Optics*, Academic Press, San Diego, Calif, USA, 2003.

[66] V. A. Belyakov, "Efficient nonlinear-optical frequency conversion in periodic media in the presence of diffraction of the pump and harmonic fields," *JETP Letters*, vol. 70, no. 12, pp. 811–818, 1999.

[67] K.-C. Shin, H. Hoshi, D.-H. Chung, K. Ishikawa, and H. Takezoe, "Enhanced second-harmonic generation by use of the photonic effect in a ferroelectric smectic C* liquid crystal," *Optics Letters*, vol. 27, no. 2, pp. 128–130, 2002.

[68] P. Palffy-Muhoray, "The nonlinear optical response of liquid crystals," in *Liquid Crystals: Applications and Uses, Vol 1*, B. Bahadur, Ed., chapter 18, World Scientific, Singapore, 1990.